

TWO-DIMENSIONAL BEAM SIZE MEASUREMENTS WITH X-RAY HETERODYNE NEAR FIELD SPECKLES

M. Siano*, B. Paroli, M. A. C. Potenza, L. Teruzzi, Università degli Studi di Milano, Milan, Italy
U. Iriso, A. A. Nosych, E. Solano, L. Torino, ALBA-CELLS, Cerdanyola del Vallés, Spain
D. Butti, A. Goetz, T. Lefevre, S. Mazzoni, G. Trad, CERN, Geneva, Switzerland

Abstract

We report on 2D beam size measurements with a novel interferometric technique named Heterodyne Near Field Speckles, capable of resolving few-micrometer beam sizes. It relies on the interference between the weak spherical waves scattered by a colloidal suspension and the intense transilluminating X-ray beam. Fourier analysis of the resulting speckles enables full 2D coherence mapping of the incoming radiation, from which the beam sizes along the two orthogonal directions are retrieved. We show experimental results obtained with 12.4 keV X-rays at the NCD-SWEET undulator beamline at ALBA, where the vertical beam size has been changed between 4 and 14 micrometers by varying the beam coupling. The results agree well with the estimated beam sizes from the pinhole calculations. Finally, we discuss recent investigations on alternative targets aimed at improving the signal-to-noise ratio of the technique.

INTRODUCTION

Two-dimensional (2D) beam size measurements are of utmost importance for present and future accelerators. Knowledge of the beam sizes enables to assess the beam emittance in storage rings [1]. Furthermore, beam size ultimately affects the transverse coherence properties of the emitted synchrotron radiation in current and forthcoming Synchrotron Light Sources (SLS), thus impacting many research areas that rely on coherence-based techniques [2].

Non-invasive beam size measurement methods can be divided into two main categories: direct imaging techniques and interferometric methods. Direct imaging techniques such as the X-ray pinhole camera directly provide a 2D image of the source, though they are typically limited in resolution to beam sizes larger than 10 μm [3]. Contrarily, interferometric methods such as the Young's double-pinhole interferometer provide higher resolutions, but are limited to one-directional measurements only [3].

Here we report on recent 2D beam size measurements with a novel, non-conventional interferometric technique named Heterodyne Near Field Speckles (HNFS). We show that the technique is intrinsically 2D and that it can resolve beam sizes as small as a few micrometers. As in all interferometric techniques, what we actually measure is the Complex Coherence Function (CCF) of the synchrotron radiation

$$\mu(\Delta\mathbf{r}) = \frac{\langle e(\mathbf{r})e^*(\mathbf{r} + \Delta\mathbf{r}) \rangle}{\sqrt{\langle i(\mathbf{r}) \rangle \langle i(\mathbf{r} + \Delta\mathbf{r}) \rangle}}, \quad (1)$$

* mirko.siano@unimi.it

from which the beam size is retrieved by means of Statistical Optics approaches. In Eq. (1), $e(\mathbf{r})$ is the electric field at a point \mathbf{r} on the wavefront of the synchrotron light, $i(\mathbf{r}) = |e(\mathbf{r})|^2$ is the corresponding intensity and $\langle \cdot \rangle$ denotes ensemble average over many electron bunches. The radiation CCF $\mu(\Delta\mathbf{r})$ quantifies the correlations of the emitted electric field between two points across the wavefront of the synchrotron light separated by $\Delta\mathbf{r}$ [4, 5].

THE HETERODYNE NEAR FIELD SPECKLES TECHNIQUE

The HNFS technique relies on the interference between the incoming partially-coherent synchrotron light and the weak spherical waves scattered by nanospheres suspended in water.

In the ideal case of a single scatterer, the self-referencing interference between the intense transilluminating field and the weak scattered spherical wave generates circular fringes whose visibility decays according to the 2D CCF of the incoming radiation, as shown in Fig. 1(a). Here, vertically elongated coherence areas have been assumed as typically encountered in undulator sources.

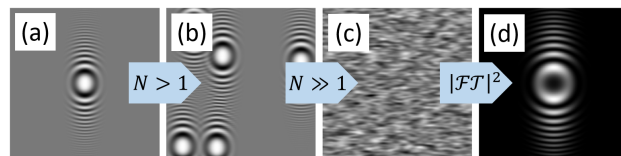


Figure 1: Fundamentals of the HNFS technique. (a) Single-particle interference image. Interference fringes are modulated by the 2D CCF of the synchrotron light. (b) and (c) Under heterodyne conditions, speckles are simply formed as the intensity sum of many equal single-particle interference patterns. (d) Power spectrum of heterodyne speckles, showing Talbot oscillations enveloped by the squared modulus of the 2D CCF.

Measurement of the visibility of the circular fringes as a function of the distance $\Delta\mathbf{r}$ from the center of the pattern allows to directly measure the 2D coherence properties of the incoming light. Furthermore, interference fringes are narrower at larger $\Delta\mathbf{r}$. This allows to introduce a one-to-one relation, known as the spatial scaling, between the spatial frequency of the interference fringes, \mathbf{q} , and transverse displacements, $\Delta\mathbf{r}$ [6–8]:

$$\Delta\mathbf{r} = z \frac{\mathbf{q}}{k}, \quad (2)$$

where z is the distance from the scattering particle and $k = 2\pi/\lambda$, being λ the radiation wavelength.

In the real case of a colloidal suspension composed by many particles, the observed intensity distribution is a random speckle pattern, as shown in Fig. 1(b,c). We assume heterodyne conditions, namely that the scattered light e_s is much weaker than the incoming field e_0 : $|e_s| \ll |e_0|$ [6–8]. In practice, heterodyne conditions for X-rays are fulfilled by properly diluting the sample to volume concentrations of roughly 10%. Under these conditions, speckles are simply formed as the intensity sum of many equal single-particle interference images as depicted in Fig. 1(b,c) and Fourier analysis of the resulting speckle patterns enables 2D coherence mapping [6–8], as evidence in Fig. 1(d). The power spectrum $I(\mathbf{q}, z)$ of heterodyne speckles at a distance z from the sample exhibits peculiar oscillations, known as Talbot oscillations, enveloped by the squared modulus of the radiation CCF [6–8]:

$$I(\mathbf{q}, z) = T(q, z)C\left(z\frac{\mathbf{q}}{k}\right)H(\mathbf{q})S(\mathbf{q}) + P(\mathbf{q}), \quad (3)$$

where \mathbf{q} denotes spatial frequencies in Fourier space, $q = |\mathbf{q}|$, $T(q, z) = 2 \sin[zq^2/(2k)]$ describes the Talbot oscillations and $C(\Delta\mathbf{r}) = |\mu(\Delta\mathbf{r})|^2$. Notice the same spatial scaling as in Eq. (2), which allows to map spatial frequencies (Fourier-space coordinates) into transverse displacements (direct-space coordinates). Terms $H(\mathbf{q})$ and $S(\mathbf{q})$ describe the additional contributions to the envelope of the Talbot oscillations due to the spatial frequency response of the detection system and the particle form factor, respectively. Finally, $P(\mathbf{q})$ describes the additive noise contribution mainly coming from shotnoise and readout noise.

THE EXPERIMENTAL SETUP AT THE NCD-SWEET BEAMLINE AT ALBA

We performed experiments at the hard X-ray undulator beamline NCD-SWEET at the ALBA Synchrotron Light Source. The experimental setup is sketched in Fig. 2.

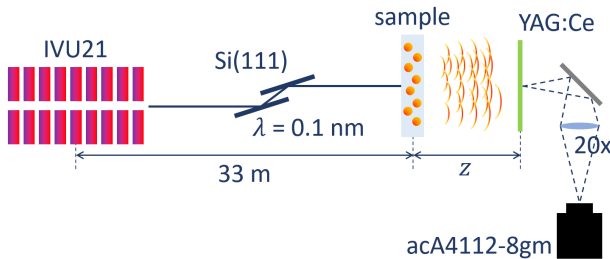


Figure 2: Experimental setup at the NCD-SWEET undulator beamline at ALBA.

A channel-cut Si(111) monochromator selects the photon energy $E = 12.4$ keV ($\lambda = 0.1$ nm), corresponding to the 7th harmonic of the IVU21 in-vacuum undulator. The X-rays impinge onto the sample consisting of a water suspension of silica spheres with diameter $d = 500$ nm, stored in 2-mm-thick capillaries at a distance $Z_0 = 33$ m downstream

the undulator center. The volume concentration of the sample is roughly 10 %, which ensures heterodyne conditions as previously mentioned. One capillary is filled with only distilled water to characterize the noise contribution $P(\mathbf{q})$. Heterodyne speckles are recorded at distances z ranging from 2 cm up to 1.2 m downstream the sample. A YAG:Ce scintillator screen with thickness 50 μm is used to convert X-ray photons into visible light. A microscope objective with nominal magnification 20x projects the visible light onto the sensor (Basler acA4112-8gm, with a pixel size of 3.45 μm). A 45-deg mirror is inserted between the scintillator and the relay optics to avoid radiation damage onto the lenses and the sensor due to the transmitted X-ray photons. For each z , we acquire a stack of 50 images to improve statistics. The acquisition frame rate is set to 1 Hz and the random Brownian motions of the sample ensure statistical independence between consecutive speckle images. The main parameters of the NCD-SWEET experimental setup are summarized in Table 1.

Table 1: Main Parameters of the NCD-SWEET Beamline

Parameter	Symbol	Value
Electron beam energy	E_{beam}	2.98 GeV
Undulator number of periods	N_w	92
Undulator period length	λ_w	21.6 mm
Photon energy	E	12.4 keV
Monochromator bandwidth	$\Delta E/E$	10^{-4}
Radiation wavelength	λ	1 \AA
Sample material		SiO ₂
Particle diameter	d	500 nm
Distance from undulator center	Z_0	33 m
Sample-detector distance	z	2 cm - 1.2 m

EXPERIMENTAL RESULTS

During the experiments, the beam coupling was varied to test the sensitivity of the technique to different beam sizes. Four different values of the beam coupling were tested: $\kappa = 0.50\%$, $\kappa = 0.65\%$ (nominal coupling during operations), $\kappa = 1.60\%$ and $\kappa = 2.80\%$. Figure 3 shows an example of the 2D power spectra acquired at the same sample-detector distance under the four different beam configurations.

Power spectra are rotated by roughly 5 degrees due to a relative tilt between the electron beam and the sensor. Nevertheless, the intrinsic 2D nature of the HNFS technique allows to unambiguously identify the horizontal and vertical beam axes regardless of such misalignment.

Qualitatively, the horizontal width of the power spectra (i.e. the horizontal coherence) is always the same for all four coupling values. On the other hand, the vertical width of the power spectra (i.e. the vertical coherence) is progressively decreasing as the beam coupling is increased. We report a direct comparison of vertical profiles in Fig. 3(e) for visual purposes. In terms of beam sizes, this implies that the hor-

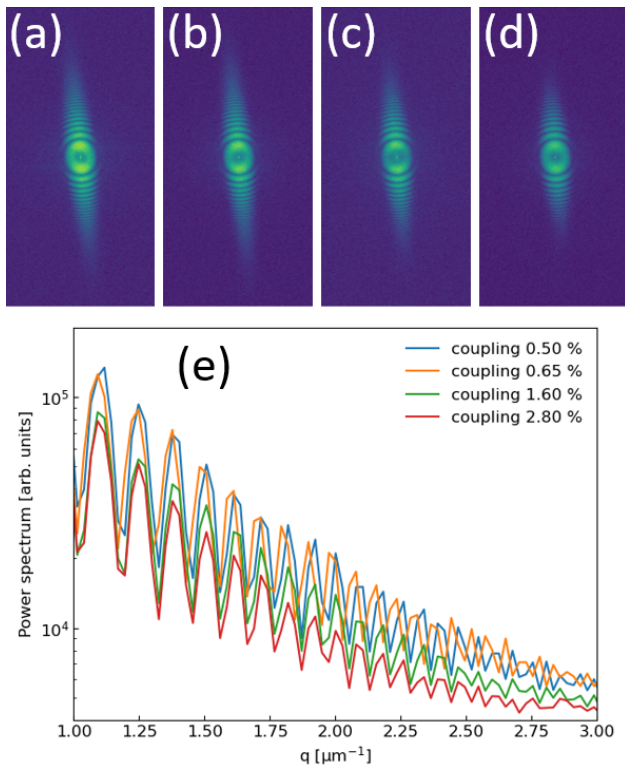


Figure 3: 2D power spectra of heterodyne speckles acquired at the same sample-detector distance under different beam couplings. (a) $\kappa = 0.50\%$, (b) $\kappa = 0.65\%$, (c) $\kappa = 1.60\%$, (d) $\kappa = 2.80\%$. (e) Direct comparison of vertical profiles.

horizontal beam size is unchanged during the coupling scan, whereas the vertical beam size increases.

Quantitative information on the horizontal and vertical coherence is extracted from the corresponding profiles of 2D power spectra. Using Eq. (3), we characterize the Talbot oscillations as follows:

$$T(q, z)C\left(\frac{q}{k}\right) = \frac{I(q, z) - P(q)}{H(q)S(q)}. \quad (4)$$

The noise term $P(q)$ is measured from the power spectrum of the capillary filled with only water. The contribution due to $H(q)S(q)$, which we will refer to as the calibration function, is determined from the envelope of the Talbot oscillations at the shortest distances. In fact, for $z \rightarrow 0$, $C(zq/k) \rightarrow C(0) = 1$, where the last equality directly comes from the definition of the radiation CCF given in Eq. (1). Therefore, from Eq. (3) we obtain

$$H(q)S(q) = \frac{I(q, z)_{z \rightarrow 0} - P(q)}{T(q, z)} \quad (5)$$

To avoid division by Talbot zeros in Eq. (5), we perform a piece-wise analysis and merge data from a few different distances, taking advantage of the fact that Talbot oscillations change with z .

Finally, coherence data from different sample-detector distances are merged upon the spatial scaling. As it can be

noticed from Fig. 4, Talbot maxima and minima collapse onto unique curves when data are plotted as a function of transverse displacements. We refer to these curves as the upper and lower envelopes of the Talbot oscillations, and their decay is then fitted by assuming a Gaussian CCF. In terms of coherence measurements, we stress that the technique is fully self-consistent and the width of the Gaussian CCF, also known as the coherence length of the radiation, is the only free parameter in the entire data reduction procedure. Inversion of data from transverse coherence lengths σ_{coh}^H and σ_{coh}^V into horizontal and vertical beam sizes σ_{beam}^H and σ_{beam}^V , respectively, is done by means of pre-computed Look-Up Tables obtained via extensive simulations [9]. Results are reported in Fig. 5 and in Table 2.

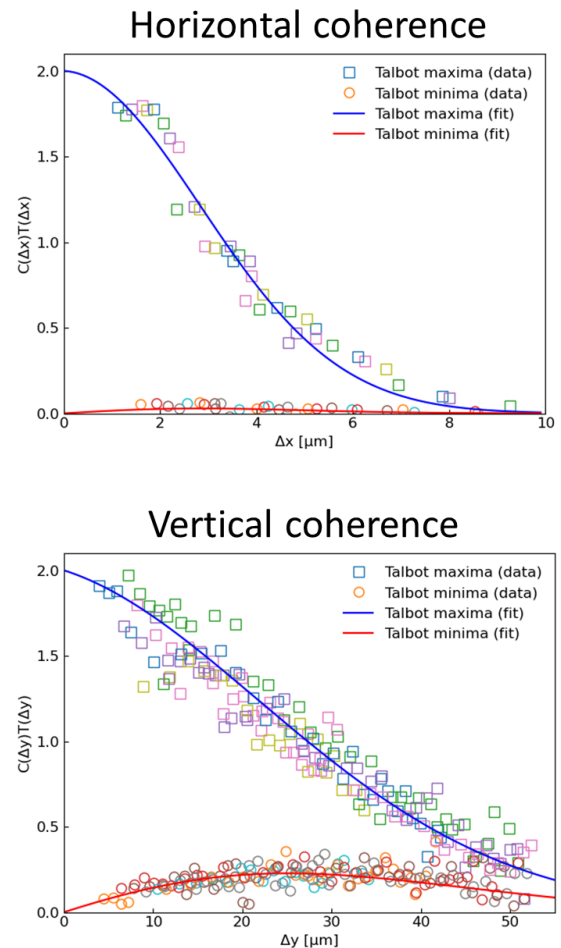


Figure 4: Talbot maxima and minima from different z collapse onto unique curves upon the spatial scaling (data refer to the case $\kappa = 2.80\%$). Their decay can be fitted assuming a Gaussian CCF to extract the coherence lengths of the radiation in the (top) horizontal and (bottom) vertical directions.

The measured horizontal beam sizes for the four different values of the beam coupling are all comparable within experimental uncertainties. The average value of $124\ \mu\text{m}$ is in good agreement with the expected value of $129\ \mu\text{m}$

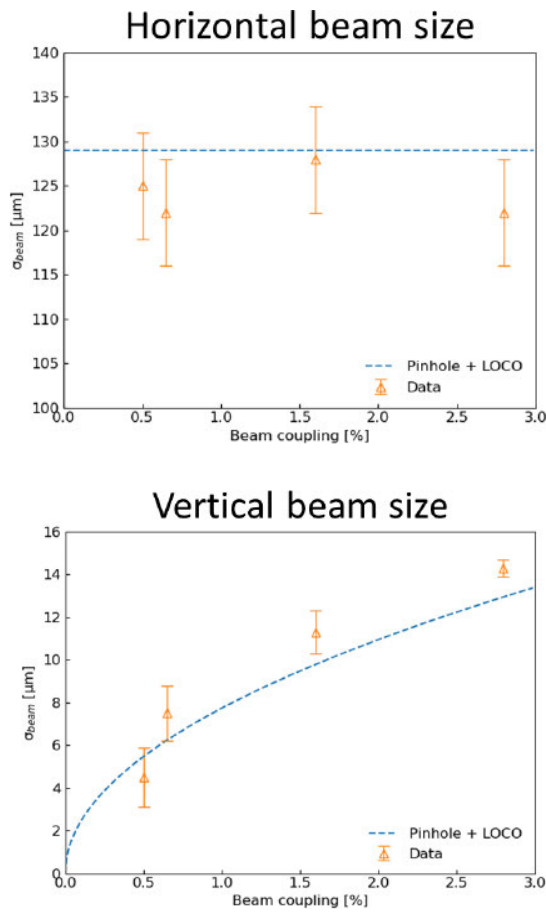


Figure 5: (Top) Horizontal and (bottom) vertical beam sizes as a function of the beam coupling.

from independent estimation based on pinhole and LOCO measurements.

At variance, the vertical beam size increases from roughly 4 μm at coupling 0.50 % to roughly 14 μm at coupling 2.80 %. Measured values are in good agreement with pinhole and LOCO estimations. Discrepancies between measured values and theoretical estimations are observed at the largest couplings, though being limited to less than 15 % (1.5 μm in absolute values). However, the model does not take into account effects, such as dispersion contributions, that might influence beam size predictions at the largest couplings. Finally, to reduce uncertainties on data at the smallest beam couplings, one should access larger sample-detector distances to better sample the high vertical coherence.

CONCLUSIONS

We have shown how the HNFS technique can be effectively used for two-dimensional electron beam size measurements. The method was tested at the NCD-SWEET undulator beamline at ALBA, where the vertical beam size was changed by varying the beam coupling in the storage ring. The measured horizontal beam size is unchanged during the coupling scan and the average value is 124 μm. Con-

Table 2: Measured coherence lengths $\sigma_{\text{coh}}^{H,V}$, measured beam sizes $\sigma_{\text{beam}}^{H,V}$ and expected beam sizes $\sigma_{\text{beam, th}}^{H,V}$ based on pinhole and LOCO estimations.

	σ_{coh}^H	σ_{beam}^H	$\sigma_{\text{beam, th}}^H$
$\kappa = 0.50 \%$	$4.2 \pm 0.2 \mu\text{m}$	$125 \pm 6 \mu\text{m}$	$129 \mu\text{m}$
$\kappa = 0.65 \%$	$4.3 \pm 0.2 \mu\text{m}$	$122 \pm 6 \mu\text{m}$	$129 \mu\text{m}$
$\kappa = 1.60 \%$	$4.1 \pm 0.2 \mu\text{m}$	$126 \pm 6 \mu\text{m}$	$129 \mu\text{m}$
$\kappa = 2.80 \%$	$4.3 \pm 0.2 \mu\text{m}$	$122 \pm 6 \mu\text{m}$	$129 \mu\text{m}$
	σ_{coh}^V	σ_{beam}^V	$\sigma_{\text{beam, th}}^V$
$\kappa = 0.50 \%$	$105 \pm 32 \mu\text{m}$	$4.5 \pm 1.4 \mu\text{m}$	$5.5 \mu\text{m}$
$\kappa = 0.65 \%$	$66 \pm 11 \mu\text{m}$	$7.5 \pm 1.3 \mu\text{m}$	$6.2 \mu\text{m}$
$\kappa = 1.60 \%$	$44 \pm 4 \mu\text{m}$	$11.3 \pm 1.0 \mu\text{m}$	$9.8 \mu\text{m}$
$\kappa = 2.80 \%$	$36 \pm 1 \mu\text{m}$	$14.3 \pm 0.4 \mu\text{m}$	$12.9 \mu\text{m}$

trarily, the vertical beam size changes from roughly 4 μm to roughly 14 μm during the coupling scan. Results along both the horizontal and vertical directions are in good agreement with expectations based on independent pinhole and LOCO measurements. For future experiments, we plan to use some gold-based sample (colloidal gold, gold glass, nanoporous gold) to increase the amount of scattered signal with respect to the current sample, thus improving the overall SNR of the technique. However, unlike the case of the silica sample, effects from the particle form factor and sedimentation should be carefully taken into account and further investigations need to be done.

REFERENCES

- [1] L. Torino, U. Iriso, “Transverse beam profile reconstruction using synchrotron radiation interferometry”, *Phys. Rev. Accel. Beams.*, vol. 19, p. 122801, 2016.
- [2] K. A. Nugent, “Coherent methods in the X-ray sciences”, *Adv. Phys.*, vol. 59, pp. 1–99, 2010.
- [3] N. Samadi, X. Shi, L. Dallin, and D. Chapman, “Source size measurement options for low-emittance light sources”, *Phys. Rev. Accel. Beams*, vol. 23, p. 024801, 2020.
- [4] J. W. Goodman, *Statistical Optics*, New York, USA, John Wiley and Sons Inc., 2000.
- [5] L. Mandel, E. Wolf, *Optical Coherence and Quantum Optics*, Cambridge, UK, Cambridge University Press, 1995.
- [6] R. Cerbino, L. Peverini, M. A. C. Potenza, A. Robert, P. Bosecke, and M. Giglio, “X-ray-scattering information obtained from near-field speckle”, *Nat. Phys.*, vol. 4, p. 238, 2008.
- [7] M. D. Alaimo, M. A. C. Potenza, M. Manfredda, G. Geloni, M. Sztucki, T. Narayanan, and M. Giglio, “Probing the Transverse Coherence of an Undulator X-Ray Beam Using Brownian Particles”, *Phys. Rev. Lett.*, vol. 103, p. 194805, 2009.
- [8] M. Siano, B. Paroli, and M. A. C. Potenza, “Heterodyne Near Field Speckles: from laser light to X-rays”, *Advances in Physics:X*, vol. 6, p. 1891001, 2021.
- [9] G. Geloni, E. Saldin, E. Schneidmiller, and M. Yurkov, “Transverse coherence properties of X-ray beams in third-generation synchrotron radiation sources”, *Nucl. Instrum. Method Phys. Res. A*, vol. 588, p. 463, 2008.